

The Optical Gravitational Lensing Experiment. Final Reductions of the OGLE-III Data*

A. Udalski, M.K. Szymański,
I. Soszyński and R. Poleski

Warsaw University Observatory, Al. Ujazdowskie 4, 00-478 Warszawa, Poland
e-mail: (udalski,msz,soszynsk,rpoleski)@astrouw.edu.pl

ABSTRACT

We describe methods applied to the final photometric reductions and calibrations to the standard system of the images collected during the third phase of the Optical Gravitational Lensing Experiment survey – OGLE-III. Astrometric reduction methods are also presented.

The OGLE-III data constitute a unique data set covering the Magellanic Clouds, Galactic bulge and Galactic disk fields monitored regularly every clear night since 2001 and being significant extension and continuation of the earlier OGLE observations. With the earlier OGLE-II and OGLE-I photometry some of the observed fields have now 16-year long photometric coverage.

Surveys – Techniques: image processing – Techniques: photometric

1 Introduction

During the third phase of the Optical Gravitational Lensing Experiment (OGLE-III), the observing capabilities of the OGLE project increased by about order of magnitude compared to the previous OGLE-II phase (Udalski, Kubiak and Szymański 1997, Szymański 2005) allowing significant extension of the sky coverage. The OGLE-III phase started on June 12, 2001 and has been continued up to now. Each clear night about 100 images (> 3 TB raw data per year) are collected with the 1.3-m Warsaw telescope equipped with eight CCD detector mosaic camera at Las Campanas Observatory, Chile (operated by the Carnegie Institution of Washington). The most important targets observed include the Magellanic Clouds, Galactic center and Galactic disk fields. The main survey is conducted for variable objects so most of observations are obtained in the I -band filter. Nevertheless, all fields are also observed from time to time in the V -band with frequency of about 10% of I -band coverage.

The observing material already collected during the OGLE-III phase is a unique dataset that can be used in a large variety of astrophysical applications. The OGLE images are obtained at one of the best observing astronomical sites worldwide so their quality – seeing, background etc. – is usually very good. However, to fully utilize their quality the state-of-the-art reduction methods must be applied. Also, the data should be precisely calibrated so they could be compared with other data sets or directly applied to astrophysical problems.

In this paper we describe reduction methods applied to the collected OGLE-III images. The main goal is to obtain the most precise, well calibrated photometry, as well as astrometry from the OGLE-III images. As the OGLE-III data will eventually be publicly available this paper can serve as a guide on the applied reduction procedures.

*Based on observations obtained with the 1.3 m Warsaw telescope at the Las Campanas Observatory of the Carnegie Institution of Washington.

2 Photometry

It was clear from the very beginning of the OGLE-III survey that the photometric reductions of the huge number of images collected during this phase should be performed in two steps: provisional on-line reductions at the telescope implemented as soon as possible after starting OGLE-III and the final reductions of the entire dataset. Because of extreme stellar density of the vast majority of fields observed by OGLE it was decided to use the DIFFERENCE IMAGE ANALYSIS (DIA) method (Alard and Lupton 1998, Alard 1999, Woźniak 2000) as the primary photometric technique used for the determination of photometry of hundreds of millions stars observed by OGLE.

The first step was implemented practically immediately after the start of the OGLE-III phase – in 2002. Because the DIA technique requires a deep, good quality reference image (usually an average of several best individual images) that serves as a template for all the remaining images it should have the possibly best resolution (lowest possible seeing) and low background. On the other hand the limited dataset of collected images after the first one/two observing seasons and urgent requirement of implementation of on-line reductions allowed construction of reference images of only moderate quality, sometimes quite far from the optimal images that could be collected with the OGLE-III hardware. Thus, the on-line OGLE-III photometry, while providing fast and still very precise magnitudes, was certainly not optimal from the photometric point of view. The OGLE-III real-time data pipeline is described in Udalski (2003).

After seven observing seasons the number of collected images during the OGLE-III phase reached almost 200 000 enough to start the huge project of re-reductions of the whole OGLE-III observing material collected so far with the goal of obtaining optimal and precisely calibrated final OGLE-III photometry.

2.1 Construction of Reference Images

The preliminary reference images used for provisional OGLE-III on-line photometry covered only the area corresponding to a single CCD detector size (2048×4096 , $0''.26/\text{pixel}$). Objects located in the gaps between neighboring detectors in the OGLE-III mosaic camera were in this way omitted. Because of imperfections in the telescope pointing the gap regions were, however, imaged from time to time. Therefore for the final reductions we decided to use extended size of the reference images: of the total size of 2180×4176 pixels, so the gaps were covered.

To construct the reference images for each field observed during OGLE-III phase a subset of good quality images for each of the subfields (corresponding to each CCD mosaic detector) of a given field was prepared. The selection of the best images was divided into two steps – automatic and manual. In the first step all available images of a given subfield were classified using various criteria: seeing, sky background level, roundness of stellar profiles and “cloudiness indicator”. The latter parameter was based on the existing provisional photometry. It can be expected that non-photometric or just cloudy nights should result in enormously large scatter of the measurements obtained during these nights. Thus, for every star brighter than $I = 18.0$ mag the mean magnitude and the standard deviation were derived, and then, for each point of each star the deviation from the mean magnitude was calculated and normalized by the standard deviation. Such coefficients were averaged over all objects in a given subfield to derive the final “cloudiness indicators”.

Only images with the seeing smaller than $1''$ ($1''.25$ for V band), the sky background smaller than 1000 ADU (300 for V band), the “roundness parameter” (defined as $1 - b/a$, where a and b are the largest and smallest diameter of stellar profile, respectively) smaller than 0.1 and the “cloudiness indicator” smaller than 1.0 were chosen to the

second step of the selection procedure. Then images were arranged according to the seeing value and they were visually inspected to reject observations with unusually bad shapes of stellar profiles, with trails of satellites, meteors or similar defects.

Up to 30 images for every subfield were selected, although every pixel of the final reference image consisted of maximum 10 the best available observations. This excess of the images was essential for preparing wide margins of the reference images.

After the standard procedure of aligning the individual subset images in the pixel grid, resampling fluxes using splines and rescaling fluxes to the scale of the first image on the subset list, each pixel of the reference image became an average of 10 or less, if not available, corresponding pixels of the best subset images. The first image on the subset list also defined the astrometric grid of the reference image.

Depending on the stellar density the photometric reductions were performed on subframes into which a subfield was divided. The most dense bulge fields in the *I*-band were divided into 545×522 pixel subframes, while much less dense *V*-band images into 1090×1044 pixel subframes. The Magellanic Cloud fields were divided either into 1090×1044 pixel subframes or into 2180×2088 pixel chunks for the less dense subfields.

2.2 Photometry

After construction of reference images all collected frames of a subfield were processed using the photometric data pipeline similar to the pipeline used in on-line reductions (Udalski 2003). The software was adjusted to handle different size of subframes.

The PSF photometry on each DIA difference image was derived for each object from the list of stellar objects on the reference image at its position on the latter. The fitting radius was set to 5 pixels. The PSF shape was derived during the transformation between a current subframe and the reference image subframe of the processed subfield in the DIA image processing. The difference flux was added to the reference image base flux of the corresponding stellar object obtained with identical photometry parameters and the total flux was converted to instrumental magnitude. Additionally the difference images were subject of the search for “new” stellar objects not associated with reference image stars. This step secured the detection of moving objects or transient objects brightening from below the detection threshold.

Each of the subframes after aligning with the corresponding reference image subframe (*i.e.*, before image subtraction) was also processed with the DOPHOT photometry program (Schechter, Saha and Mateo 1993) running in the standard “non-fixed position” mode. In this way independent PSF profile photometry of each object was derived, supplemented with astrometric information (current *X, Y* position) obtained *via* PSF fitting. The zero point of the PSF photometry was adjusted to the zero point of the DIA photometry of a given subframe by comparison of appropriate DIA and PSF magnitudes of several dozen brightest stars in each subframe.

Finally, the files containing the DIA and PSF photometry for each subframe as well as files containing “new” objects were merged into the final photometry file set for a given subfield image.

2.3 OGLE-III Photometric Databases

After processing the entire dataset of images for a given field the instrumental photometry databases enabling easy handling of so huge amount of data were constructed. The same databases as in the previous phases of the OGLE survey were used. For technical details the reader is referred to Szymański (2005) and Szymański and Udalski (1993).

Because the OGLE-III dataset of images is still open and the databases will be supplemented with photometry from further observing seasons the standard “integer” data format was used. Nevertheless all OGLE-III databases will be converted to much faster “sequential” format when the OGLE-III phase ends.

The DIA photometric databases are constructed separately for each of the subfields of a given field. They contain the following information for each object detected in the reference image: epoch – Heliocentric Julian Date of the mid-exposure, magnitude, magnitude error from the DIA reductions, photometry flags (*e.g.*, the detection of object on difference image for fast identification as possible variable), position on the reference image. The database of “new” objects contains similar information. However, the brightness and its error for these objects are kept in flux units.

Additional PSF reduction procedure described in the previous Section enabled construction of independent PSF photometric databases. Although the PSF photometry is generally more noisy in the dense stellar fields it may be necessary for correct identification of variable objects and in some cases for more precise photometric calibration of the DIA photometry.

The PSF databases were also constructed separately for each subfield and their structure is similar to the DIA photometry database. However, each record for a given epoch, in addition to the photometric data (magnitude, PSF magnitude error), contains also (X, Y) position of the object on this frame. In this way the PSF databases enable fast retrieving of not only photometric but also astrometric data of a given object (*cf.* Section 3.1). Because the detection level of stars processed by the PSF photometry pipeline strongly depends on the seeing of a frame the number of detected stars varies from image to image of the same field. Thus, the cross-identification of detected objects is a necessary step before feeding the PSF database records. Fortunately, the pixel grid of all reduced images is the same (they are aligned with the DIA reference image before processing), so the cross-identification is straightforward: objects located within 1.9 pixel ($0''.5$) radius from the reference image position are treated as associated with a given reference image stellar object. One has, however, be aware that some high proper motion stars can leave such an aperture after some time.

2.4 Calibration

During the first couple of years of the OGLE-III project the collected images were reduced photometrically in the real time at the telescope and the photometry was immediately fed into databases for easy data handling. This provisional photometry was only roughly calibrated based on very approximate zero points derived by comparison of stellar magnitudes in OGLE-II fields observed in the course of the OGLE-III survey. Accuracy of zero points of photometry was only about ± 0.1 – 0.2 mag. Although that accuracy of absolute calibration was certainly not sufficient for many projects, these data were fully useful for all applications studying stellar variability.

Huge amount of data, large field of the sky covered by the images and very dense stellar fields observed by OGLE make the standard system precise calibration a difficult task. Here, we describe our methods of calibrating OGLE-III photometry based on calibrations of the Magellanic Cloud images. At the moment of writing this paper, the Galactic bulge data are still being reprocessed. However the procedures that will be applied to this latter data set will be practically identical.

Photometric Flatness of OGLE-III Images

The first step in the procedure of calibrating the OGLE-III data was the determination of the photometric flatness of each of the mosaic camera images. Systematic spatial trends were encountered during calibration of OGLE-II data and one could expect similar scale or larger effects present in the OGLE-III images. This could be an effect of imperfections in flat fielding, changing scale in the camera field and other systematic effects.

To derive the maps of the flatness we conducted a dedicated observing program carried out on 12 photometric nights during the years 2007–2008. We observed the Landolt’s standard fields (PG2213-006 and RUBIN 149; Landolt 1992) in nine positions on each chip: left, middle and right in X -axis and bottom, middle and top in the Y -axis. To ensure accurate measurements the seeing could not exceed 7 pixels. Measurements were obtained in both V and I -band filters.

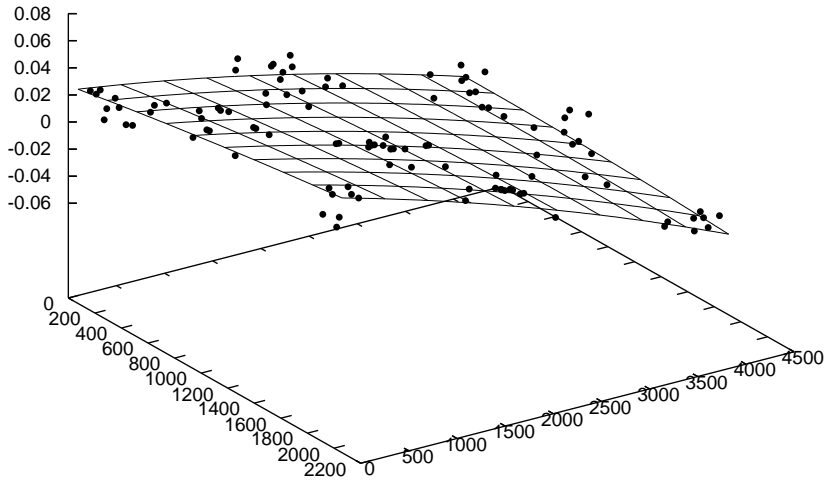


Fig. 1. Flatness map derived from observations of standard stars for OGLE-III subfield #2.

After collecting the data, magnitudes of standard stars were measured with the aperture photometry with the radius of 14 pixels. Then we normalized the magnitudes of each star taking as the zero point magnitude of this standard star located in the center of the image for a given observing dataset. In this way we obtained a map of the measured magnitudes relatively to the chip center. Such maps were constructed for each chip and each observing night. Finally we fitted a surface $\Delta\text{mag} = f(X, Y)$ to all individual maps for each chip. The residuals of the typical surface fit were of the order of 0.015 mag.

As one could expect there are systematic changes of photometric signal across the detectors. They are, however, very stable and can be accurately mapped by our fitted surfaces. Fig. 1 shows the flatness map for one of the OGLE-III mosaic chips.

Observations of Photometric Standard Fields

OGLE-II phase photometric data were calibrated to the standard system using the Landolt’s (1992) standard fields observed on several dozen photometric nights. To ensure homogeneity we adopted similar strategy in OGLE-III phase and the same standard fields were supposed to be used as the main calibrators. However, it soon turned out that the calibration of each individual chip of the OGLE-III mosaic camera on many photometric nights would be an extremely time consuming task limiting the time available for scientific observations. As a result the standard fields were observed relatively

rarely and often the standards were observed on single chip only. Nevertheless, during the course of the OGLE-III phase the Landolt fields were observed on more than 30 photometric nights during the years 2003–2008 allowing determination of accurate transformation of the instrumental magnitudes to the standard system. Calibration of photometry of each particular chip to the standard system could be derived on more than 20 photometric nights.

All standard stars in the observed fields were measured using aperture photometry with the aperture radius of 14 pixels. Then the magnitudes were corrected for the photometric flatness of respective chip using maps described above. Next, for each chip, the mean nightly transformations in the form:

$$V = v + k_V \cdot X + \varepsilon_V \cdot (V - I) + ZP_V$$

$$I = i + k_I \cdot X + \varepsilon_I \cdot (V - I) + ZP_I$$

were derived, where lowercase letters describe aperture instrumental magnitudes normalized to one second exposure time, k denotes the extinction coefficient, X – air mass, ε – color term coefficient and ZP – the zero point of the transformation.

T a b l e 1

Color term coefficients for the OGLE-III subfields

Subfield	ε_V	ε_I
Chip 1	-0.039 ± 0.010	0.050 ± 0.016
Chip 2	-0.038 ± 0.008	0.040 ± 0.017
Chip 3	-0.036 ± 0.010	0.042 ± 0.019
Chip 4	-0.045 ± 0.010	0.044 ± 0.015
Chip 5	-0.040 ± 0.009	0.043 ± 0.011
Chip 6	-0.039 ± 0.011	0.040 ± 0.015
Chip 7	-0.037 ± 0.014	0.039 ± 0.015
Chip 8	-0.043 ± 0.007	0.044 ± 0.012

It turned out that the color term transformation coefficients behaved quite stable over the several years long observations during the OGLE-III phase. Therefore we decided to average the derived values of these coefficients for the future use with the final databases. Table 1 lists the adopted ε coefficients for each chip.

Calibration of the OGLE-III Fields with Standard Stars

Only a small fraction of the OGLE-III fields could be calibrated directly with the observations of standard stars, because of limited number of nights when the standard fields were observed. Nevertheless we performed such a calibration to compare calibrated magnitudes with independent data set, namely OGLE-II photometry, and in this way we could double check consistency of the applied procedures.

Calibration of the OGLE-III instrumental photometry to the standard system with observations of the standard stars was performed in the following steps. First, the aperture corrections to instrumental magnitudes from the DIA data pipeline were derived. Because of high stellar density of the vast majority of the OGLE-III fields a special procedure was developed. Each of the subframes on which the DIA photometry had been derived was analyzed independently. On each of them 7–170 brightest stars (in the Magellanic Cloud fields) with no companions of comparable brightness within the radius of 20 pixels were selected as stars for aperture correction determination. Then the customary program based on the DOPHOT photometry program was run on each

of the subframes. First, it derived the PSF photometry of all objects on the subframe. Then it subtracted from the original subframe all the stars except the ones on the aperture correction list, minimizing in this way contamination of aperture stars by fainter neighbors. Finally it calculated the aperture correction for each star from the aperture correction star list by subtracting its aperture magnitude measured in 14 pixel aperture on so prepared cleaned image from the DIA magnitude obtained with the pipeline reductions. The median value of the aperture corrections from all selected stars was taken as the final aperture correction of a given subframe. Aperture corrections were calculated for all OGLE-III fields observed on “standard stars” nights.

Then, the offset between the DIA instrumental magnitudes and standard system was calculated for each subframe for a given “standard stars” night. The offset included the aperture correction, one second exposure normalization, extinction term, $k \cdot X$, and the zero point value for a given night (as obtained from standard stars observations). The average of these offsets from all standard nights was then used as the calibration shift between OGLE-III instrumental and standard systems. Such a correction does not include the color term, $\epsilon \cdot (V - I)$, which is individual for each object.

Comparison with OGLE-II Photometry

To compare the standard stars calibration of the OGLE-III photometry with independently calibrated OGLE-II dataset we cross-identified all OGLE-II stars with OGLE-III counterparts based on astrometric solutions (see Section 3.2). Only OGLE-III subfields (corresponding to an individual detector image of a given OGLE-III field) with overlap larger than 75% with OGLE-II fields were used in this test. Also, for comparisons only the brighter stars were selected: $V < 19$ mag and $I < 18$ mag, with standard deviation of all measurements smaller than 0.04 mag.

78 and 53 subfields in the LMC were suitable for comparison of the OGLE-III and OGLE-II photometry in the I and V bands, respectively (they fulfilled overlap criteria and were calibrated with standard stars). Unfortunately none of the OGLE-III SMC fields that overlap with OGLE-II were observed in the V filter on the “standard stars” nights, so in the SMC only I -band photometry could be compared (48 subfields). Altogether 622 272 LMC stars were used for comparison of OGLE-III standard star calibration with OGLE-II photometry in the I -band and 698 847 in the V -band. In the SMC 117 743 stars were compared in the I -band.

OGLE-II calibrated magnitudes were taken from the LMC and SMC photometric maps (Udalski *et al.* 1998, 2000). The OGLE-III instrumental magnitudes were shifted using the calibration offsets described above, corrected for photometric flatness and for the color term, using OGLE-II $V - I$ color and average color coefficients (Table 1). The shifts between the OGLE-III and OGLE-II magnitudes of all selected common stars were then calculated.

The median shift between the OGLE-III and OGLE-II magnitudes was determined for each subframe of each analyzed subfield and the average value for each subfield was calculated. The final difference of the OGLE-III photometry calibrated directly with standard stars and OGLE-II photometry, calculated as the mean of all comparison subfields in a given OGLE-III target and filter, and its standard deviation is listed in Table 2.

As it can be seen from Table 2 the agreement between the OGLE-III and OGLE-II magnitudes is extremely good. Practically the shifts between both datasets are negligible what is reassuring and indicates that the calibration procedures are self consistent. This also indicates that the huge OGLE-II dataset can serve as the large set of secondary standard stars enabling simple and easy way of calibration of all OGLE-III fields. Practically on each night several OGLE-III fields that overlap with OGLE-II ones have been observed during the OGLE-III survey providing calibrating standards

Table 2

Mean difference between OGLE-III photometry calibrated directly with standard stars and OGLE-II photometry

LMC <i>I</i> -band:	-0.004 ± 0.013	71 subfields
LMC <i>V</i> -band:	-0.003 ± 0.013	53 subfields
SMC <i>I</i> -band:	$+0.004 \pm 0.013$	48 subfields

for the remaining OGLE-III fields.

Finally, the shifts between OGLE-III and OGLE-II photometry of hundreds of thousands stars from all overlapping subfields were used for the determination of second order spatial corrections to the first approximation correction for photometric flatness obtained from measurements of standard stars. Huge sample of common stars distributed uniformly over entire chips allowed more precise mapping of low level trends than limited standard stars measurements.

First, to minimize the possible low level systematic errors in the OGLE-II maps (resulting from the reduction and calibration methods of OGLE-II drift-scan images) the shifts of all common stars were plotted as a function of *X* position of a star in the OGLE-II image. Then the mean shift level as a function of OGLE-II *X* coordinate was fitted with splines and OGLE-II magnitudes were detrended (*i.e.*, shifts were corrected; the correction was always in the range $(-0.014, 0.010)$ mag). Finally, the mean values of so adjusted shifts in appropriate pixels of each OGLE-III mosaic chip were found and the chip surfaces were smoothed forming second order photometric flatness correction maps of each mosaic detector.

Establishing the Set of OGLE-II Standards

Results of the comparison of OGLE-III standard stars calibrated photometry with OGLE-II photometry imply that the OGLE-II photometry can be used as the set of secondary standards for calibrating purposes. Therefore, for the final calibrations of OGLE-III photometry we selected a set of OGLE-III subfields that overlap with OGLE-II fields on more than 75%. Altogether 92 such subfields from 23 OGLE-III fields in the LMC and 48 subfields from 11 OGLE-III SMC fields were selected as “photometric calibrators”.

Before we started calibration procedures using OGLE-II fields, we prepared lists of ten best images of all observed OGLE-III fields. In the *I*-band we used the same criteria as in the selection of frames for construction of the reference images (seeing $< 1''$, background < 1000 ADU), but this time we sorted images according to the “cloudiness indicator” and selected images with the lowest value of this parameter (usually smaller than 0.6). Because of much smaller number of *V*-band images and general observing strategy that *V*-band observations are taken on “photometrically looking” nights all *V*-band observations with seeing smaller than $1''.5$ were considered as the best images.

All nights when the best images were taken, supplemented by the nights when the photometric conditions were confirmed by observations of standard stars, were assumed to be “calibrating nights”. All observations of “photometric calibrators” taken on these nights were used for the determination of zero points for a given night. Standard deviation of the zero points derived from different “photometric calibrators” subfields served as the consistency check of the photometric condition of a night. Only the nights when $\sigma_{ZP} < 0.03$ mag were considered as photometric.

The OGLE-III DIA pipeline photometry of the “photometric calibrators” subfields was color term corrected based on the OGLE-II color index, corrected with aperture correction derived for each subframe, extinction corrected and compared with OGLE-II photometry. The median of the magnitude shifts for the brightest stars (fulfilling similar magnitude and error limitations as in the previous Subsection) was considered as the photometric scale zero point. Independent determinations from different calibrators were then averaged and their scatter served as the measure of the photometric quality of the night.

Altogether about 180 photometric nights for each of the mosaic CCD detectors calibrated using the OGLE-II LMC and SMC “photometric calibrators” were used for calibration of the *I*-band images and about 130 for *V*-band ones.

As another consistency check we compared the *I*-band zero points derived with OGLE-II “photometric calibrators” with direct determinations using standard stars described above. The mean difference of the zero points obtained with the two methods was found to be: -0.001 ± 0.017 mag for 92 common determinations. This confirms full agreement of the OGLE-II calibration approach with classical calibration method using standard stars.

Final Calibration of the OGLE-III Photometry

With the determination of the zero points of OGLE-III photometry on so many photometric nights using OGLE-II “photometric calibrators”, it became possible to calibrate all the remaining OGLE-III fields. First, for all LMC and SMC images taken on “calibrating nights” the aperture corrections were derived using procedure described previously. Then for each subframe in a given subfield photometric offsets as in the calibration with standard stars were calculated using just derived zero point for a given night. Finally, the average offsets from all nights for each subframe were determined after removing two extreme (largest and smallest) values in the *I*-band and one extreme value in the much smaller *V*-band set. Typical number of individual offsets averaged for a subfield was 64 and 34 for the SMC and LMC *I*-band data and 22 and 12 for *V*-band observations, respectively. The typical scatter of individual offsets around the mean value was about 0.010 mag.

Correction of Databases

In the final step the databases containing the OGLE-III photometry in the instrumental system were adjusted in such a way that the final OGLE-III database of a given subfield for a given band contains calibrated magnitudes of each object except for the color term, $\epsilon \cdot (V - I)$, because no color information about the object is *a priori* known. The correction to photometry of each object included the flatness correction, the second order flatness correction – both dependent on the position of the star in a subfield – and the mean offset for a subframe of a given subfield. Because the PSF instrumental photometry was tied during the reduction procedure to the DIA photometry, the same corrections apply to the same object in the DIA and PSF databases.

To calculate calibrated OGLE-III photometry of a given star one has to obtain a color information on the object to correct database magnitudes for the color term. If this object is present in the other band OGLE-III database the procedure is straightforward: one should extract and then calibrate the $(v - i)$ instrumental color according to the following equation:

$$(V - I) = (v - i) / (1 - \epsilon_V + \epsilon_I)$$

and then apply the color term correction using the transformation color coefficients for a given chip provided in Table 1. When a star does not have OGLE color information one can assume a typical color of the population of stars in the analyzed sample. Accuracy will be somewhat lower, but on the other hand the color term is a second order

correction so the inaccuracy of such an approximation should be small.

Figs. 2–9 present a few examples of the comparison of OGLE-III calibrated photometry with the OGLE-II Photometric Maps for subfields from the center and outer regions of the galaxy bar in the I and V -band. One can see that the residual differences and/or some residual trends are small, at most of the order of 0.01–0.02 mag, *i.e.*, practically negligible. These small trends are mostly noticeable as a function of OGLE-III Y coordinate, *i.e.*, the OGLE-II X coordinate and seem to be correlated with OGLE-II subframe division. Thus their origin is likely related to small systematic effects in the OGLE-II calibration.

3 Astrometry

CCD images can be successfully applied to astrometric applications. Good resolution quality of OGLE images obtained at Las Campanas Observatory – one of the best observing sites worldwide – makes this material very attractive for astrometric applications. Indeed the OGLE-II images were successfully used for construction of the proper motion catalogs of the Magellanic Cloud and Galactic bulge line-of-sight objects (Soszyński *et al.* 2002, Sumi *et al.* 2004). OGLE-III images are even more attractive for astrometric purposes as the finer sampling of $0''.26/\text{pixel}$ is better suited to the typical observing seeing conditions. Astrometry from OGLE-III should be then more precise than from OGLE-II frames.

3.1 Astrometric Databases

The PSF photometric databases described in Section 2.3 can also serve as astrometric databases. They contain current (X, Y) position of each object detected in the DIA reference image on every collected OGLE-III image. This position is derived by PSF fitting (X, Y, flux) with the DOPHOT program after aligning the current image with the reference image and transformation to the same pixel grid. Astrometric databases provide then direct access to proper motion measurements of a given object in X and Y coordinates. X and Y axes of the OGLE-III images are roughly aligned with N-S and E-W directions, respectively. Fig. 10 shows OGLE-III data of an exemplary high proper motion object taken from Soszyński’s *et al.* (2002) catalog.

3.2 Transformation of Pixel Coordinates to the Equatorial System

The astrometric transformation of the OGLE-III pixel grid coordinates to the equatorial system was performed in similar way as in the previous phases of the OGLE project (Udalski *et al.* 1998) with some modifications required to allow for much larger area covered by the OGLE-III observations, including fields of significantly lower star density.

Each subfield of the OGLE-III targets, corresponding to a single chip of the mosaic CCD camera had its astrometric transformation computed independently. Then stars were cross-identified in the overlapping regions of the neighboring reference images and their RA/DEC coordinates computed from two independent transformations were compared as the test for the accuracy of the astrometric calibration. Typical error estimated by this comparison was about $0''.06$. This test was made much simpler than in former OGLE phases after introducing reference images which cover larger area than the single chip of the CCD camera.

The procedure of finding the coordinates transformation for each subfield was performed in following steps. As the preparation, the lists of brightest stars in the subfield

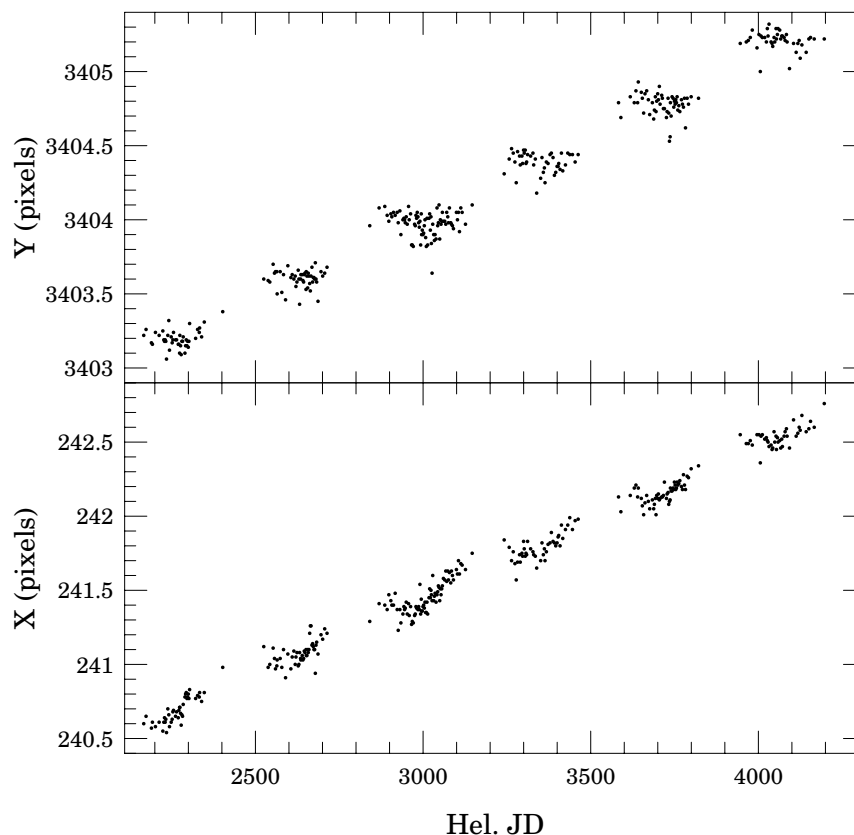


Fig. 10. Astrometry of high proper motion object LMC_SC13 351-352 (Soszyński *et al.* 2002). One pixel corresponds to $0''.26$.

were extracted from the OGLE database and from the chosen external catalog. A few catalogs were tested, including the Second USNO CCD Astrograph Catalog (UCAC2, Zacharias *et al.* 2004), the Catalog of Astrometric Standards USNO-A2.0 (Monet *et al.* 1998) and the Two Micron All Sky Survey (2MASS) Point Source Catalog (Skrutskie *et al.* 2006). The best of these, for the purpose of finding our transformation, proved to be the 2MASS Catalog and it was uniformly used for all fields in the Magellanic Clouds.

In the second step, a short list of identified stars and a preliminary transformation between the X, Y pixel coordinates from the OGLE database and the RA/DEC from the 2MASS Catalog list was found using the WCSTools software package (Mink 2002).

In the last step, the third-degree polynomial transformation was calculated using as many stars from both lists as we could cross-identify. The same algorithm was used as in previous phases of the OGLE project, thus allowing to add the results to the common OGLE database of astrometric transformations and to use the same software. The transformations were carefully tested for uniformity and accuracy, as explained above.

4 Summary

OGLE-III databases constitute a unique dataset containing long term time series photometry of hundreds of millions stars. The targets observed during the OGLE project,

namely the Magellanic Clouds and the Galactic center are very important from the astrophysical point of view thus making these databases especially attractive for data mining and statistical analysis of large samples of objects of different types.

In this paper we presented technical details on processing the collected images to derive the most precise and well calibrated photometry. Also details on astrometric reductions were provided.

The finally reduced OGLE-III data will be gradually released to public domain. Information on the available data sets can be found at:

<http://ogle.astrouw.edu.pl>

Acknowledgements. This paper was partially supported by the Polish MNiSW grants: N20303032/4275 to AU and NN203293533 to IS and by the Foundation for Polish Science through the Homing Program.

This publication makes use of data products from the Two Micron All Sky Survey, which is a joint project of the University of Massachusetts and the Infrared Processing and Analysis Center/California Institute of Technology, funded by the National Aeronautics and Space Administration and the National Science Foundation.

REFERENCES

- Alard, C., and Lupton, R. 1998, *Astrophys. J.*, **503**, 325.
 Alard, C. 2000, *Astron. Astrophys. Suppl. Ser.*, **144**, 363.
 Landolt, A.U. 1992, *Astron. J.*, **104**, 372.
 Mink, D.J. 2002, in: *ASP Conf. Ser.* **281**, "Astronomical Data Analysis Software and Systems XI", Ed. D.A. Bohlender, D. Durand, and T.H. Handley (San Francisco: ASP), 169.
 Monet, D., *et al.* 1998, USNO-SA2.0: "A Catalog of Astrometric Standards (Washington: US Nav. Obs.).
 Schechter, P.L., Saha, K., and Mateo, M. 1993, *P.A.S.P.*, **105**, 1342.
 Skrutskie, L.M. *et al.* 2006, *Astron. J.*, **131**, 1163.
 Soszyński, I., Żebruń, K., Udalski, A., Woźniak, P.R., Szymański, M., Kubiak, M., Pietrzyński, G., Szewczyk, O., and Wyrzykowski, Ł. 2002, *Acta Astron.*, **52**, 143.
 Sumi, T., Wu, X., Udalski, A., Szymański, M., Kubiak, M., Pietrzyński, G., Soszyński, I., Woźniak, P., Żebruń, K., Szewczyk, O., and Wyrzykowski, Ł. 2004, *MNRAS*, **348**, 1439.
 Szymański, M., and Udalski, A. 1993, *Acta Astron.*, **43**, 91.
 Szymański, M.K. 2005, *Acta Astron.*, **55**, 43.
 Udalski, A. 2003, *Acta Astron.*, **53**, 291.
 Udalski, A., Kubiak, M., and Szymański, M. 1997, *Acta Astron.*, **47**, 319.
 Udalski, A., Szymański, M., Kubiak, M., Pietrzyński, G., Woźniak, P., and Żebruń, K. 1998, *Acta Astron.*, **48**, 147.
 Udalski, A., Szymański, M., Kubiak, M., Pietrzyński, G., Soszyński, I., Woźniak, P., and Żebruń, K. 2000, *Acta Astron.*, **50**, 307.
 Woźniak, P.R. 2000, *Acta Astron.*, **50**, 421.
 Zacharias, N., Urban, S.E., Zacharias, M.I., Wycoff, G.L., Hall, D.M., Monet, D.G., and Rafferty, T.J. 2004, *Astron. J.*, **127**, 3043.

Captions of JPEG figures.

Fig. 2. Difference between the *I*-band OGLE-III calibrated photometry and OGLE-II photometry for common stars from the central bar subfield LMC100.1. *Upper panel* shows the difference as a function of *X* image coordinate (N-S direction) while the *lower panel* as a function of *Y* coordinate (E-W direction).

Fig. 3. Same as Fig. 2 for the bar subfield LMC111.2.

Fig. 4. Same as Fig. 2 for the western part of the bar subfield LMC126.1.

Fig. 5. Same as Fig. 2 for the eastern part of the bar subfield LMC177.3.

Fig. 6. Same as Fig. 2 for the *V*-band.

Fig. 7. Same as Fig. 3 for the *V*-band.

Fig. 8. Same as Fig. 4 for the *V*-band.

Fig. 9. Same as Fig. 5 for the *V*-band.

This figure "fig2.jpg" is available in "jpg" format from:

<http://arxiv.org/ps/0807.3884v1>

This figure "fig3.jpg" is available in "jpg" format from:

<http://arxiv.org/ps/0807.3884v1>

This figure "fig4.jpg" is available in "jpg" format from:

<http://arxiv.org/ps/0807.3884v1>

This figure "fig5.jpg" is available in "jpg" format from:

<http://arxiv.org/ps/0807.3884v1>

This figure "fig6.jpg" is available in "jpg" format from:

<http://arxiv.org/ps/0807.3884v1>

This figure "fig7.jpg" is available in "jpg" format from:

<http://arxiv.org/ps/0807.3884v1>

This figure "fig8.jpg" is available in "jpg" format from:

<http://arxiv.org/ps/0807.3884v1>

This figure "fig9.jpg" is available in "jpg" format from:

<http://arxiv.org/ps/0807.3884v1>